

# AEROELASTIC ANALYSIS OF THE NASA/ARMY/MIT ACTIVE TWIST ROTOR

W. Keats Wilkie

Matthew L. Wilbur

Paul H. Mirick

*Army Research Laboratory  
NASA Langley Research Center  
Hampton, VA 23681*

Carlos E. S. Cesnik

SangJoon Shin

*Active Materials and Structures Laboratory  
Massachusetts Institute of Technology  
Cambridge, MA 02139*

## ABSTRACT

Aeroelastic modeling procedures used in the design of a piezoelectric controllable twist helicopter rotor wind tunnel model are described. Two aeroelastic analysis methods developed for active twist rotor studies, and used in the design of the model blade, are described in this paper. The first procedure uses a simple flap-torsion dynamic representation of the active twist blade, and is intended for rapid and efficient control law and design optimization studies. The second technique employs a commercially available comprehensive rotor analysis package, and is used for more detailed analytical studies. Analytical predictions of hovering flight twist actuation frequency responses are presented for both techniques. Forward flight fixed system  $nP$  vibration suppression capabilities of the model active twist rotor system are also presented. Frequency responses predicted using both analytical procedures agree qualitatively for all design cases considered, with best correlation for cases where uniform blade properties are assumed.

## INTRODUCTION

A means of accomplishing individual blade control without the need for complex mechanisms in the rotating system has been sought for many years. Recently, many electromechanical approaches exploiting active (smart) material actuation mechanisms have been investigated for this purpose.<sup>1</sup>

The most widely explored active material actuation methods have employed either piezoelectrically actuated flaps placed at discrete locations along the blade,<sup>2-7</sup> or piezoelectric material distributed along the blade and used to directly control deformations (usually twist) in the host blade structure.<sup>8-17</sup> The primary design constraint in both approaches is the need to obtain high piezoelectric actuation forces and displacements with a minimum of actuator weight. An additional concern with flap actuation mechanisms is that they must be designed to fit within the geometric confines of the blade structure. Direct control of blade twisting using embedded piezoelectric materials, although simple conceptually, has also proven to be difficult to implement. This is chiefly due to the high stiffnesses of rotor blades in torsion, and restrictions in energy densities and bandwidth capabilities of currently available active materials.

Although twist deformation control of rotor blades is very difficult to achieve, recent analytical and experimental investigations have indicated that piezoelectric *active fiber composites* (AFC) imbedded in composite rotor blade structures, may be capable of meeting the performance requirements necessary for a useful individual blade control system.<sup>10-17</sup> The active fiber composite actuator utilizes interdigitated electrode poling (IDE)<sup>18</sup> and piezoelectric fiber composites (PFC),<sup>19</sup> as shown in Fig. 1. This combination results in a high performance piezoelectric actuator laminate with strength and conformability characteristics greater than that of a conventional monolithic piezoceramic.<sup>20</sup> In particular, the high conformability of the actuator package allows it to be embedded easily within nonplanar structures, much like a traditional composite ply.

---

*Presented at the American Helicopter Society 55<sup>th</sup> Annual Forum, Montreal, Canada, May 25-27, 1999. This paper is declared a work of the U.S. Government and is not subject to copyright protection in the United States.*

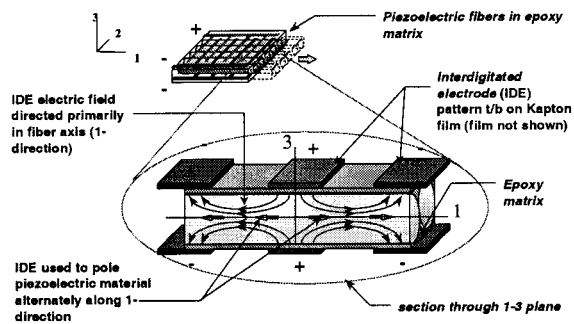


Figure 1. Active Fiber Composite piezoelectric actuator concept.

Buoyed by encouraging analytical results, several experimental efforts examining the practical potential of active fiber composites for rotor individual blade control are now underway. The first of these is a collaborative effort between Boeing and the Massachusetts Institute of Technology.<sup>11, 13, 16, 17</sup>

This effort, sponsored by the Defense Advanced Research Projects Agency (DARPA), has successfully completed a preliminary hovering flight test of a single 1/6 scale CH-47D model blade incorporating AFC twist actuation.<sup>16, 17</sup> Results from this test are currently being used to design a three-bladed 1/6 scale rotor system for eventual Mach-scaled wind tunnel testing in air.

An additional experimental program, the NASA/ARL/MIT Active Twist Rotor project (ATR), is also underway. As part of this effort, a Mach and Froude scaled AFC actuated wind tunnel model will be constructed and tested in the NASA Langley Transonic Dynamics Tunnel (TDT).<sup>21</sup> The TDT utilizes a heavy gas test medium with a speed of sound approximately one half that of air. This allows full-scale blade Mach numbers to be attained at rotational speeds much lower than those required for Mach-scaled models operating in air. The lower rotor speeds also generally reduce blade stresses, which relaxes many model design constraints.

Demonstrating the AFC twist actuation concept at full-scale blade stresses, a much more difficult challenge and a necessary precursor to eventual flight testing, will be performed in the as part of the DARPA integral twist test program. In the interim, the ATR is expected to provide an important first wind-tunnel demonstration of the active fiber composite rotor concept, and will serve as a basic experimental research platform for controllable twist research and control law design.

Appropriate analytical tools are necessary for any design effort. For the Active Twist Rotor project, a variety of mathematical and computational methods were employed to arrive at the final ATR

design. In this paper, the computational methods used to predict the aeroelastic behavior of the Active Twist Rotor, and intermediate designs, will be discussed. In addition to an overview of these methodologies, analytical predictions of hovering flight active twist frequency responses and forward flight vibration reduction capabilities for the ATR model rotor will be presented. The sensitivities in these analytically predicted results due to various aeroelastic modeling assumptions will also be examined.

## AEROELASTIC MODELING OF ACTIVE TWIST ROTORS

Two numerical active twist rotor modeling approaches have been developed at NASA Langley Research Center. The first, the Piezoelectric Twist Rotor Analysis (PETRA), has been developed using the MATLAB numerical analysis package,<sup>22</sup> and is specifically intended for fundamental studies of active twist rotor designs with embedded actuators. The second approach employs the commercially available CAMRAD II comprehensive rotor analysis package<sup>23</sup> and is used for more detailed analytical studies. Both active twist rotor blade aeroelastic modeling approaches are described below.

### PETRA ACTIVE TWIST ROTOR AEROELASTIC ANALYSIS

The Piezoelectric Twist Rotor Analysis (PETRA) computer program is a simple numerical aeroelastic analysis code designed for rapid and efficient control law and design optimization studies. A complete description of the theory underlying the mathematical model is given in Ref. 14. The primary components and features of PETRA are described below.

The blade equations of motion used in PETRA are adapted from the second degree nonlinear equations of Kaza and Kvaternik.<sup>24</sup> These equations are simplified to a linear out-of-plane bending-torsion model through the use of an ordering scheme applicable to rotor blade vibration studies. Blade structural properties, including piezoelectric actuation terms, were determined using the sectional analysis methods described in Ref. 25. The resulting generalized piezoelectric actuation forces are applied to the right hand side of the final equations of motion along with all aerodynamic forcing terms.

The aerodynamic loads acting on the rotating blade are derived using strip theory and a finite-state unsteady aerodynamics formulation, which includes the ONERA model of dynamic stall.<sup>26-28</sup> For simplicity, a uniform inflow model, with a linear

variation across the rotor disk in forward flight is used. Airfoil parameters used in the finite-state model are based on the “generic” rotorcraft airfoil described in Ref. 26. Although not an exact match to any specific airfoil, these properties form a good qualitative representation of a typical modern rotorcraft airfoil. Quasisteady compressibility effects are also accounted for in the airfoil parameters.

As the stall aerodynamic terms are highly nonlinear, a numerical time integration procedure is used to obtain a solution to the aeroelastic equations of motion in forward flight. This is first accomplished by obtaining a system of ordinary differential equations using a modified Galerkin procedure and then integrating these equations in the time domain using a MATLAB-based numerical analysis procedure. The polynomial bending and torsion comparison functions developed by Karunamoorthy and Peters<sup>29</sup> are used when applying the Galerkin procedure in PETRA, although any suitable comparison functions may be used. A numerical autopilot technique is also used during the time integration process to obtain trimmed, steady state flight conditions.<sup>30</sup> This enables vibratory loads for active twist blades and conventional passive structure blades to be compared equally under identical flight conditions.

For hovering flight cases an alternative solution approach is available. This procedure uses a linearized system of equations developed about a steady-state hovering flight solution. This approach is particularly useful for control and stability studies and is easily used with traditional eigenanalysis techniques. For convenience, this approach was used for the PETRA results presented in this paper.

### CAMRAD II MODELING

While the PETRA active twist rotor analysis is a very useful preliminary design tool, more extensive rotorcraft modeling capabilities were also desired for development of the Active Twist Rotor model. Early in the design stages of the ATR, the second generation version of the Comprehensive Analytical Model of Rotorcraft Aerodynamics and Dynamics (CAMRAD II) was introduced for detailed numerical studies of the active twist rotor concepts. In particular, the sophisticated wake models available with CAMRAD II permit more general analytical vibration reduction studies to be performed.

CAMRAD II does not directly provide a method for introducing piezoelectric actuation effects into the rotor blade structure. However, by taking advantage of the modeling flexibility built into the code, such a method was easily developed. A CAMRAD II model is typically created from ‘shell’ inputs. Detailed model definitions and revisions are often necessary

and can be defined using the more detailed ‘core’ input capability. This is illustrated schematically in Fig. 2. Here core modeling has been utilized to impose a torsional couple to the blade structural model generated by the CAMRAD II shell. The lower box in Fig. 2, in which all hub and joint modeling has been omitted for clarity, shows the finite element model of a single ATR blade. The upper box in the figure shows the harmonic twisting loads that are defined by user input. These harmonic loads are converted to the time domain by a CAMRAD II ‘Fourier Series’ component. The resulting twist control vector is applied to the blade tip and the joint between finite element beams 1 and 2 with opposite unity gains to complete the active twist control modeling.

### ACTIVE TWIST ROTOR BLADE AEROELASTIC DESIGN

The primary consideration for design of the ATR was the unique test environment of the Langley Transonic Dynamics Tunnel. The TDT utilizes a heavy gas test medium (R134a) with a speed of sound approximately one half that of sea-level standard air. This, along with the TDT’s variable density test capability, permits full scale rotor tip Mach numbers, Froude numbers, and Lock numbers to be matched simultaneously at approximately one-quarter model scale. In particular, the reduced speed of sound in the heavy gas medium allows full-scale tip Mach numbers to be matched at lower rotational speeds, with typically lower blade stresses.

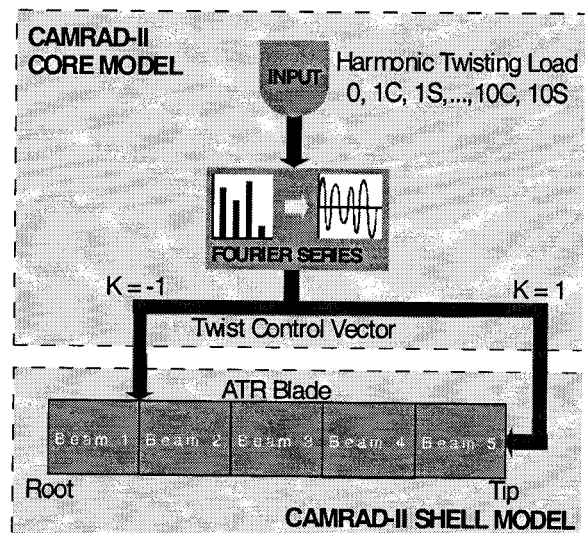


Figure 2. CAMRAD II dynamic model schematic for the ATR blade.

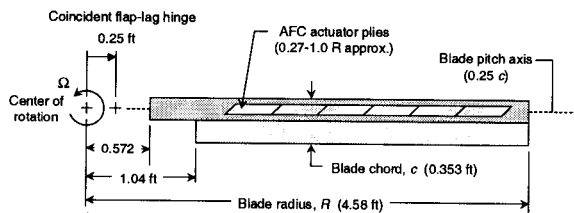
**Table 1. Comparison of nondimensional main rotor blade parameters.**

parameter	UH-1D	CH-46	H-34	S-61	CH-53	CTR	ATR
$EI_{fw}/m\Omega^2 R^4$	2.95E-03	3.32E-03	1.92E-03	2.22E-03	3.30E-03	1.92E-03	<b>2.61E-03</b>
$EI_{cw}/m\Omega^2 R^4$	8.97E-02	9.77E-02	2.09E-02	2.30E-02	9.97E-02	2.09E-02	<b>7.25E-02</b>
$GJ/m\Omega^2 R^4$	2.36E-03	1.78E-03	2.36E-03	3.11E-03	1.77E-03	2.30E-03	<b>2.36E-03</b>
$M_{tip}$	0.740	0.627	0.591	0.599	0.633	0.545	<b>0.600</b>
$c/R$	0.0729	0.06	0.0488	0.0491	0.06	0.0488	<b>0.0773</b>
$\sigma$	0.0464	0.0573	0.0621	0.0781	0.115	0.0621	<b>0.0984</b>
$\gamma$	7.7	8.9	9.8	9.2	12.4	8.3	<b>9.0</b>

These factors combined to provide considerable latitude in the design of the ATR model.

A prototype ATR model rotor blade for use with a 4-bladed articulated rotor hub on the ARES rotorcraft test system was recently constructed at the MIT Active Materials and Structures Laboratory (AMSL).<sup>31</sup> The prototype ATR blade will be used for nonrotating bench tests and single active blade spin tests to evaluate the ATR design and construction methods. After completion of these tests, a set of four ATR model blades based on the prototype design will be constructed for wind tunnel testing.

As the ATR is intended to be a basic active twist research platform, an uncomplicated blade planform, twist distribution, and airfoil distribution, was desired. Also, to reduce cost of blade manufacture, it was advantageous to utilize existing model blade tooling as much as possible. With these constraints in mind, a suitable set of blade molds from those available at NASA Langley Research Center were identified and selected for use in the construction of the ATR prototype blade. The ATR blade planform and dimensions are shown in Fig. 3. Dimensions, twist, and airfoil do not match any particular vehicle, but are reasonably representative of a typical production helicopter rotor blade. A comparison of nondimensional blade properties for the ATR and



- NACA 0012 airfoil contour from station 12.5 to blade tip
- -10° built-in linear twist from center of rotation to blade tip

Figure 3. ATR model blade planform.

nondimensional full-scale values for several typical helicopters is shown in Table 1. A listing of ATR design parameters used in the analytical studies in this paper is provided in the Appendix. A detailed description of the design, fabrication, and bench testing of the ATR prototype blade is given in Ref. 31.

A cutaway drawing illustrating the structural geometry of the prototype Active Twist Rotor model blade is shown in Fig. 4. Structural design of the active twist blade was accomplished using an asymptotic formulation for the analysis of multi-cell composite beams incorporating imbedded piezoelectric plies. Flapwise, chordwise and torsional design limit loads were determined using CAMRAD II analytical results, and based on an assumed wind tunnel limit flight condition of  $C_l/\sigma = 0.075$ ,  $C_D/\sigma = -0.0066$ , and  $\mu = 0.36$ . Exact details of the beam formulation used in the design of the ATR prototype blade are given in Ref. 25.

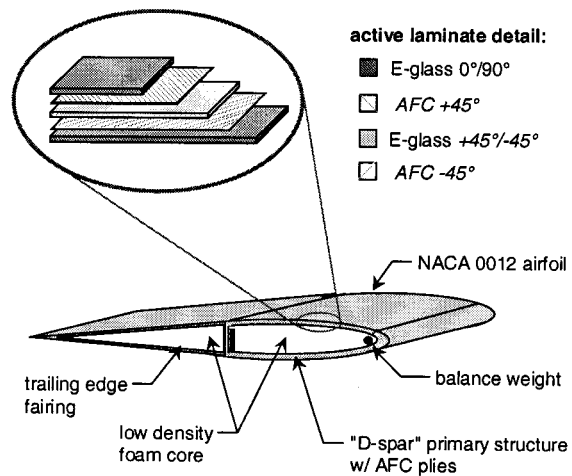


Figure 4. ATR blade spar structure.

As indicated in Fig. 4, AFC laminae are embedded in the blade structure at alternating  $\pm 45^\circ$  orientation angles which maximizes the twist actuation capabilities of the active plies. With an even number of AFC plies, it is also possible to keep the passive structure of the rotor blade elastically uncoupled.

## RESULTS

In developing the final Active Twist Rotor design, a variety of results were generated using both the PETRA and CAMRAD II modeling procedures. Samples of fanplot, frequency response, and forward flight vibration reduction results obtained for two different representations of the ATR are presented here. The first version represents a uniform blade property ATR design generated before detailed blade fabrication techniques were considered directly. This design will be referred to as the "development" design. The second version more closely represents the final ATR design, and includes nonuniform structural and piezoelectric actuation properties. This design will be referred to as the "final" design. For all cases, blade structural properties, including piezoelectric twist actuation moments, as determined by the MIT blade section analysis methods, were used.<sup>32,33</sup>

### ATR DEVELOPMENT DESIGN

The development design of the ATR consists of a blade with uniform properties from blade root to tip. For the PETRA models the blade root is placed at the center of rotation with a spring on the flap hinge simulating the effects of hinge offset. For the CAMRAD II model the blade root is placed outboard of the pitch bearing, at approximately 0.10R. For both the PETRA and CAMRAD II models the active twist region is assumed to extend from the blade root to the blade tip.

The PETRA results shown were obtained using linear constant coefficient system matrices calculated for each hovering flight case. Five bending comparison functions and five torsional comparison functions, given in Ref. 29, were used in the Galerkin procedures for all cases. States associated with the aerodynamics formulation were evaluated at 20 spanwise locations along the blade (five system states per point), distributed from the root cutout to the tip, with a greater concentration of the evaluation points toward the tip. Steady state values, required for generating the constant coefficient hovering flight system matrices, were obtained by specifying a blade

collective pitch setting and then numerically iterating upon the blade equations of motion with all state derivatives set to zero. Hovering flight blade dynamics, as determined by the resulting system matrices, were then examined using the standard linear time invariant system analysis tools available with MATLAB.

The CAMRAD II models include a fully coupled flap-lag-torsion-axial blade representation using five finite element beams each of which have 15 degrees-of-freedom, including six rigid and nine elastic degrees-of-freedom. During the analysis procedure a modal solution is implemented which reduces the system degrees-of-freedom to 12 dynamic and 28 quasistatic blade modes. No other system degrees-of-freedom, including fixed-system flexibility, have been modeled. The 4-bladed articulated hub components consist of rigid elements with a lag-flap universal joint placed at 0.055R and a pitch bearing at 0.108R. Rotor system trim control is achieved through once-per-revolution actuation of the pitch bearing; thus no swashplate control system is modeled.

### IN VACUO BLADE FREQUENCIES

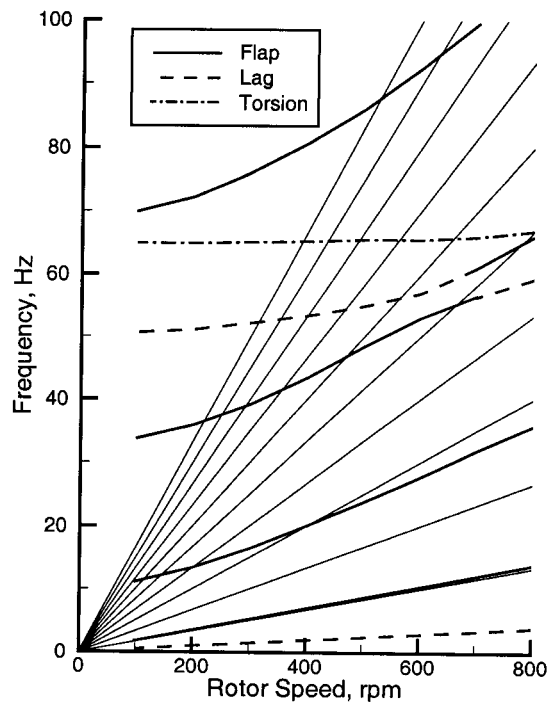
A fanplot of the ATR development design blade frequencies is presented in Fig. 5 for both the PETRA and CAMRAD II models. As shown, good agreement exists between the two models. Table 2 presents the in vacuo blade frequency results at the ATR design speed of 687.5 rpm.

**Table 2. In vacuo per revolution modal frequencies for the ATR development model ( $\Omega_0 = 687.5$  RPM).**

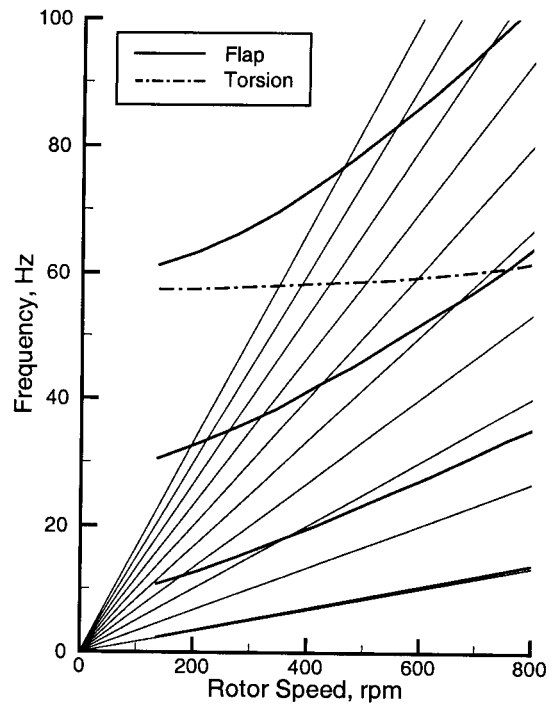
Mode	PETRA	CAMRAD II
Rigid Lag	----	0.29
Rigid Flap	1.02	1.04
Elastic flap 1	2.67	2.72
Elastic flap 2	4.99	4.91
Elastic lag 1	----	5.28
Elastic torsion 1	4.92	5.76
Elastic flap 3	8.32	8.60

### HOVERING FLIGHT TWIST ACTUATION FREQUENCY RESPONSE

Predicted twist actuation frequency response for the ATR final design is shown in Fig. 6 for a nominal 1g ( $C_L/\sigma = 0.075$ ) hovering flight condition. For these results a uniform inflow distribution was assumed for both analyses. Agreement between the



(a) CAMRAD II results.



(b) PETRA results.

Figure 5. ATR development design fanplots.

two analytical methods is extremely good, and shows that the fundamental active twist rotor dynamics are being modeled consistently. The ATR development blade is predicted by both analysis methods to achieve static twist actuation amplitudes of 2 to 2.5 degrees. Hovering flight dynamic twist actuation amplitudes of approximately 4 degrees are predicted for the frequency range of 3P to 5P.

#### FORWARD FLIGHT VIBRATION REDUCTION CASE STUDY

One of the goals of the Active Twist Rotor program is to provide new research for the development of low vibration rotor concepts. As such, a considerable effort was expended to identify the vibration reduction characteristics of the ATR. For this work the CAMRAD II model of the ATR development design was used to determine the effect of 3P, 4P, and 5P blade twist actuation on 4P fixed-system vibratory loads. The CAMRAD II model is an isolated rotor configuration without the flexibility or inertial characteristics of the fixed-system represented. Therefore, the results presented are for the loads imposed by the ATR blades on an infinite impedance hub. All of the results presented in this section have been calculated with a free wake model

and are for a constant forward flight velocity,  $\mu = 0.30$ , at a 1g trim condition of  $C_{l}/\sigma = 0.075$  and

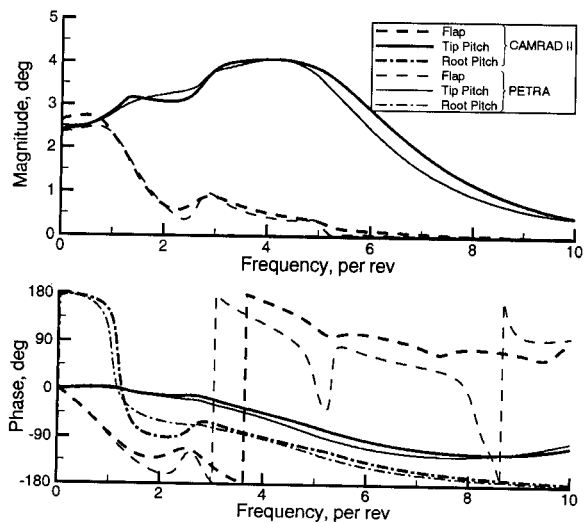


Figure 6. ATR development design twist actuation frequency response. Hovering flight ( $\Omega_0 = 687.5$  rpm,  $C_{l}/\sigma = 0.075$ ).

$C_D/\sigma = -0.0046$ . A maximum twisting control moment of 1.01 ft-lb, as calculated by PETRA, was assumed.

Figures 7, and 9 through 12 present a set of contour plots describing some of the calculated 4P fixed-system loads obtained for the ATR development design under 3P, 4P, and 5P control. The plots are presented with the applied twist actuation control phase plotted on the x-axis and the applied twist actuation control amplitude on the y-axis. The contours present the resulting 4P fixed-system load generated by the corresponding twist actuation control phases and amplitudes. Thus, the contour levels at the bottom of the plots (along the x-axis) where the control amplitude is zero represent the baseline load condition generated by the ATR without any twist actuation applied. As one moves up the plots an increasing control amplitude is applied. As one moves left and right on the plots the actuation phase is varied. The figure captions indicate the baseline (no actuation) load and the minimum load obtained.

Figure 7 presents the calculated results for the 4P vertical hub shears,  $F_z$ , due to 4P twist actuation. As shown, significant reductions or increases in vertical shear are predicted depending upon actuation amplitude and phase. The minimum 4P vertical hub shear of 1.39 lb is predicted at an amplitude of 0.3 ft-lb and phase of  $330^\circ$ . This represents a reduction of 76% when compared to the unactuated 4P vertical hub shear of 5.68 lb. It is noteworthy that only 30% of the actuation twist authority is necessary to obtain the minimum load result. Actuation amplitudes of 0.5 ft-lb and greater consistently resulted in higher fixed-system loads for all cases (shears and moments) due to the increasing inertial loads inherent in the actuation of the blade. Thus, the ATR is predicted to be over-designed from a control authority standpoint.

Figure 8 presents the results from figure 7 in a different manner. This figure directly shows the 4P vertical hub shear as a function of twist actuation phase for five different actuation amplitudes.

As expected, the greatest effect on fixed-system lateral shears and overturning moments was generally predicted for 3P and 5P twist actuation. Figures 9 and 10 present the contour plots for 3P and 5P actuation respectively and their effect on 4P fixed-system side force. As shown in Fig. 10, 5P actuation is predicted to have a relatively minor effect on 4P fixed-system side force when compared to the significant gradients shown in the other contour plots. However, this is somewhat deceiving as 5P twist actuation is predicted to achieve as much as a 63% reduction in the side force. Twist actuation at 3P is predicted to reduce side forces by up to 88% as shown in Fig. 9.

Figures 11 and 12 present the 4P fixed-system rolling moment response to 3P and 5P twist actuation respectively. Predicted results show a reduction in 4P rolling moment of 88% for 3P actuation and 92% for 5P actuation.

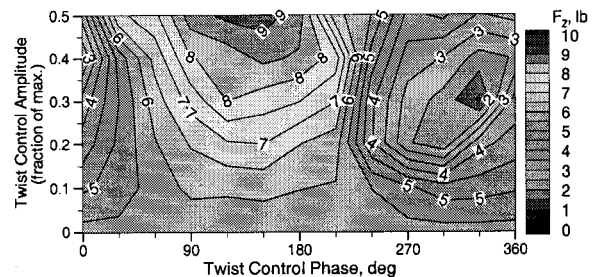


Figure 7. Predicted 4P vertical hub shear due to 4P twist actuation. Baseline  $F_z = 5.68$  lb. Minimum  $F_z = 1.39$  lb.

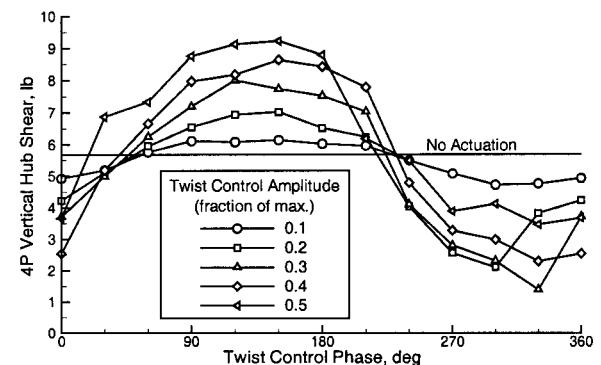


Figure 8. Comparison of predicted 4P vertical hub shear due to 4P twist actuation and amplitude variation.

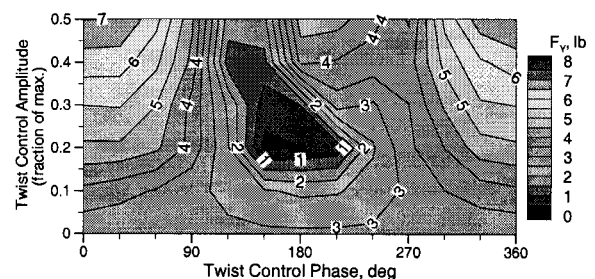


Figure 9. Predicted 4P fixed-system side force due to 3P twist actuation. Baseline  $F_y = 3.10$  lb. Minimum  $F_y = 0.37$  lb.

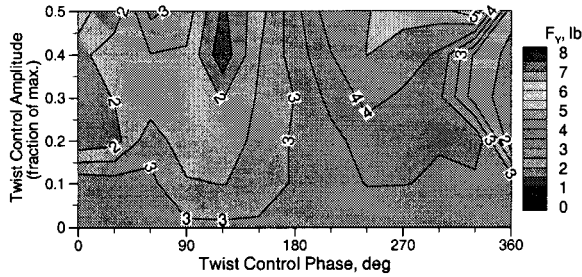


Figure 10. Predicted 4P fixed-system side force due to 5P twist actuation. Baseline  $F_Y = 3.10$  lb. Minimum  $F_Y = 1.15$  lb.

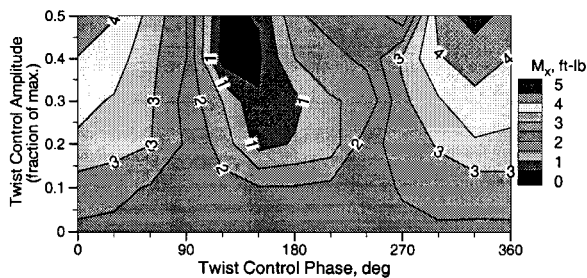


Figure 11. Predicted 4P fixed-system rolling moment due to 3P twist actuation. Baseline  $M_X = 2.40$  ft-lb. Minimum  $M_X = 0.28$  ft-lb.

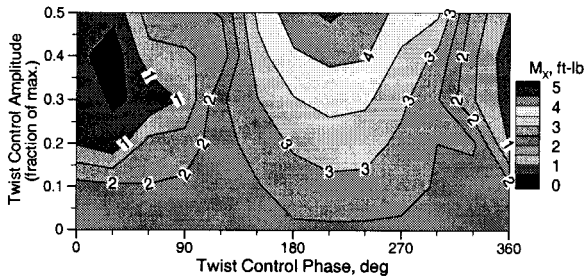


Figure 12. Predicted 4P fixed-system rolling moment due to 5P twist actuation. Baseline  $M_X = 2.40$  ft-lb. Minimum  $M_X = 0.20$  ft-lb.

### FINAL ATR DESIGN CASE STUDIES

The final design of the ATR incorporates the structural properties of the blades to be fabricated. This includes a region of elevated stiffness from the blade root to 0.27R. As noted previously, the elevated stiffness region extends from the center of rotation to 0.27R for the PETRA model, and from the pitch bearing (0.108R) to 0.27R for the CAMRAD II model.

### IN VACUO BLADE FREQUENCIES

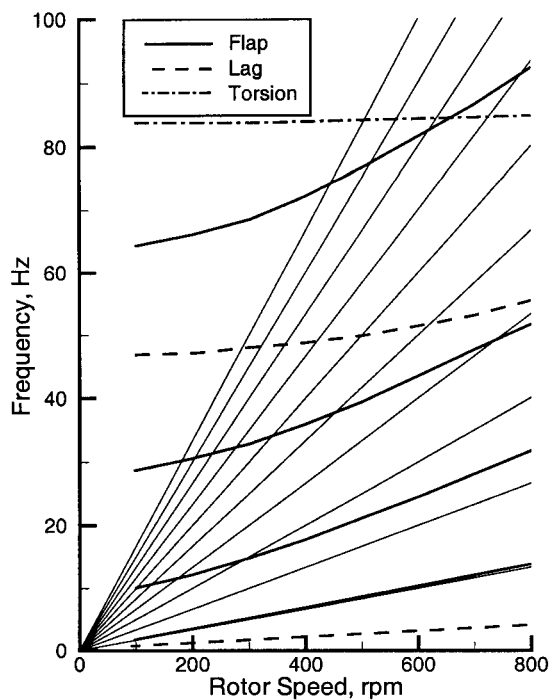
A fanplot of the ATR final design blade frequencies is presented in Fig. 13 for both the PETRA and CAMRAD II models. Table 3 presents the in vacuo blade frequency results at the ATR design speed of 687.5 rpm. As shown, reasonably good agreement exists between the two models at lower blade frequencies, although the higher frequencies modes tend to show more pronounced differences. These discrepancies are thought to be due to the limited number of torsional and bending comparison functions (five of each) used with the PETRA model. Five comparison functions were seen to generate good results with uniform blades, although a greater number of functions is probably required to generate acceptable results with nonuniform blades, particularly those with large spanwise property variations.

**Table 3. In vacuo per revolution modal frequencies for the ATR final design model ( $\Omega_0 = 687.5$  RPM).**

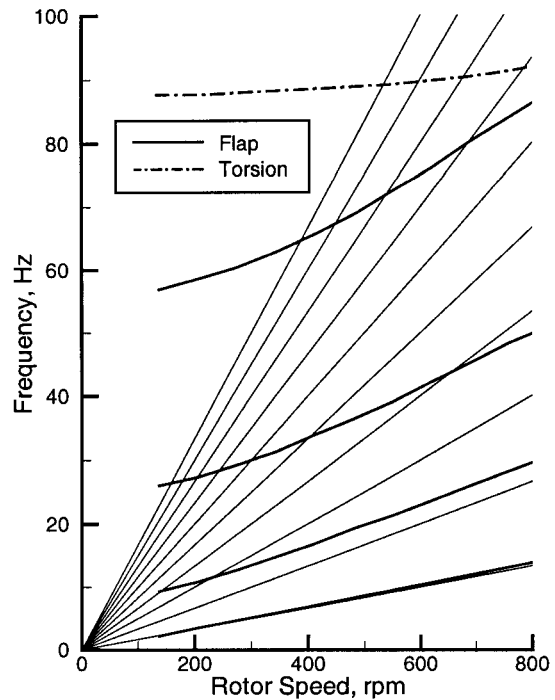
Mode	PETRA	CAMRAD II
Rigid Lag	----	0.33
Rigid Flap	1.03	1.05
Elastic flap 1	2.26	2.41
Elastic flap 2	3.94	4.13
Elastic lag 1	----	4.61
Torsion 1	7.87	7.37
Elastic flap 3	6.98	7.50

### HOVERING FLIGHT TWIST ACTUATION FREQUENCY RESPONSE

Predicted twist actuation frequency responses for the ATR final design are shown in Fig. 14 for the nominal 1g ( $C_L/\sigma = 0.075$ ) hovering flight condition. For these results a uniform inflow distribution was assumed for both the PETRA and CAMRAD II models. Agreement in twist amplitude between the two methods is not as good as with the ATR development model, but the general characteristics of the response are similar. Note that twist actuation phase is practically identical for both methods. Again, the quantitative discrepancies seen between the PETRA and CAMRAD II cases are most likely due to the numerically stiffer first torsion mode predicted with PETRA. Both methods predict a relatively high degree of dynamic twist actuation authority for the ATR design, despite the reduced spanwise coverage of actuation plies.



(a) CAMRAD II results.



(b) PETRA results.

Figure 13. ATR final design fanplots.

Figure 15 compares the predicted active twist frequency responses as a function of hover thrust. The conditions shown are the 1g design lift ( $C_L/\sigma = 0.075$ ), and lifting tasks above ( $C_L/\sigma = 0.095$ ) and below ( $C_L/\sigma = 0.055$ ) the 1g flight condition. Flap response differences were minimal and were not plotted. Figure 15 shows that minimal differences in response are expected due to changes in rotor thrust condition. The PETRA model, in fact, shows virtually no response differences due to thrust. This was expected as the aerodynamics representation used in PETRA is essentially linear below stall conditions. The CAMRAD II model indicates minor differences in response for the highest thrust case. In general, both modeling methods predict that thrust does not significantly affect twist actuation frequency response for hovering flight conditions away from stall.

Figure 16 compares the predicted frequency responses for the ATR as functions of rotor speed. Three rotor speed cases are shown: the ATR at its nominal design speed and lifting condition ( $\Omega_0 = 687.5$  rpm,  $C_L/\sigma = 0.075$ ), the ATR at a higher rotational speed ( $1.1\Omega_0$ ), and the ATR at a lower rotational speed ( $0.9\Omega_0$ ). Both modeling methods predict similar trends on the active twist frequency

response with changes in the reduced torsional frequency of the blade. These trends, in addition to illustrating the importance of blade reduced torsional frequency on active twist performance, also seem to indicate a large degree of coupling with blade bending response. This is evidenced most notably in the flattening of the twist actuation frequency response as the per-revolution torsional frequency approaches the first and second elastic flap modes in the 3P to 5P range. The degree to which this coupling may be exploited in the design of active twist rotor systems remains to be fully explored.

The sensitivity of active twist frequency response predictions to the type of inflow model chosen in the analysis was examined with CAMRAD II. (PETRA at present contains a uniform inflow model only.) Figure 17 compares the predicted frequency response generated using a prescribed wake model to the response generated using uniform inflow. Minimal differences in response are shown, with the exception of flap response below 1P, which for the prescribed wake case increased by approximately 25% over the uniform inflow case. For design purposes, the use of uniform inflow seems to be adequate for estimating hovering flight twist actuation response.

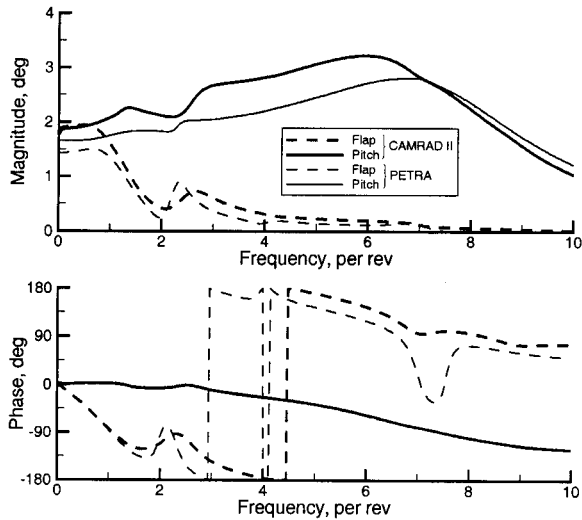


Figure 14. ATR final design twist actuation frequency response. Hovering flight ( $\Omega_0 = 687.5$  rpm,  $C_l/\sigma = 0.075$ ).

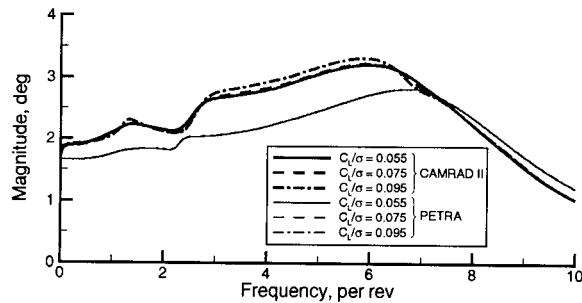


Figure 15. Effect of rotor thrust on hovering flight active twist frequency response ( $\Omega_0 = 687.5$  rpm).

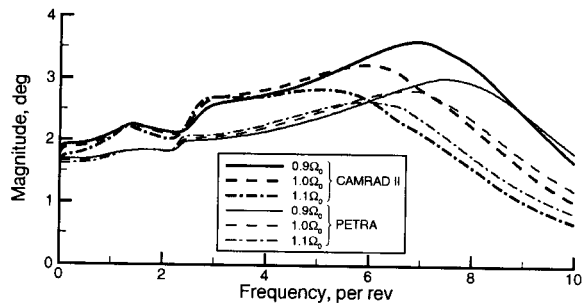


Figure 16. Effect of rotor speed on hovering flight active twist frequency response ( $\Omega_0 = 687.5$  rpm,  $C_l/\sigma = 0.075$ ).

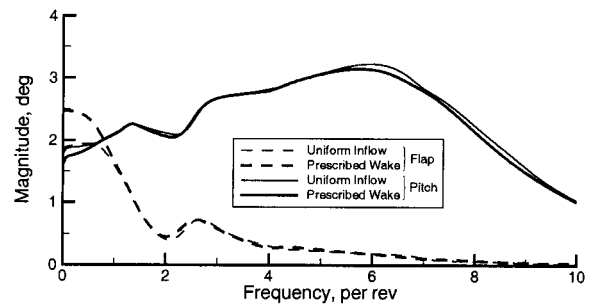


Figure 17. Effect of inflow model on hovering flight active twist frequency ( $\Omega_0 = 687.5$  rpm,  $C_l/\sigma = 0.075$ ). CAMRAD II results only.

## CONCLUSIONS

Two aeroelastic modeling approaches have been utilized to study piezoelectric active twist rotor systems. The first, PETRA, utilizes a simplified mathematical model, and is design for use with the MATLAB numerical analysis package. The second employs the commercially available CAMRAD II code. Design cases used in the development of the NASA/Army/MIT Active Twist Rotor system have been studied using both approaches. Results with both approaches are in consistently good agreement.

Experimental data to compare with the analytical trends shown here will soon be forthcoming. A prototype ATR blade, based on the final design parameters used here, was recently completed at the Massachusetts Institute of Technology, and a hovering flight test is expected to begin soon at the NASA Langley Research Center. A follow-on forward flight wind tunnel test of the complete four-bladed Active Twist Rotor system is scheduled for early 2000.

The conclusions of this study are summarized below:

1. High static and dynamic twist actuation authority, in excess of two degrees amplitude, is predicted by both approaches for the NASA/ARL/MIT Active Twist Rotor model.
2. Hovering flight frequency response predictions using both approaches are in excellent agreement for the ATR development design, where uniform blade properties were assumed.
3. Frequency response predictions for the ATR final design, with structurally nonuniform blade properties, are in qualitatively good agreement using both approaches.
4. Calculated hovering flight frequency responses for both modeling approaches were relatively insensitive to rotor thrust.

5. Both modeling approaches displayed similar frequency response characteristics with rotor speed variation, and indicate that torsional frequency placement is a critical design consideration for active twist rotor systems.

6. Calculated hovering flight frequency responses using CAMRAD II were relatively insensitive to the wake model utilized.

7. Forward flight simulations using CAMRAD II indicate that large reductions in 4P vertical hub shear may be achievable with significantly less than the maximum twist actuation authority of the Active Twist Rotor.

#### APPENDIX: ACTIVE TWIST ROTOR BLADE PARAMETERS

**Table A1. Active Twist Rotor general parameters.**

property	description	value
$R$	Blade radius, ft	4.58
$c$	Blade chord, ft	0.353
$r_c$	Root cutout, ft	1.04
$\theta_{pt}$	Blade linear pretwist, deg	-10
$N$	Number of blades	4
$e$	Flap-lag hinge location, ft	0.25
$\Omega_0$	Nominal rotor rotational speed, RPM	687.5
$\rho_0$	Nominal test medium density, slug/ft <sup>3</sup>	0.00472
$M_{tip}$	Blade tip Mach number	0.60

**Table A2. Active Twist Rotor structural properties: development design.**

property	description	value
$m$	Section mass per unit length, slug/ft	1.47E-02
$I_\theta$	Section polar mass moment of inertia, slug-ft <sup>2</sup> /ft	8.70E-05
$EA$	Axial stiffness, lb	3.13E+05
$EI_{fw}$	Flapwise stiffness, lb/ft <sup>2</sup>	8.67E+01
$EI_{cw}$	Chordwise stiffness, lb/ft <sup>2</sup>	2.41E+03
$GJ$	Torsional stiffness, lb/ft <sup>2</sup>	7.84E+01
$Q_{PE}$	Maximum piezoelectric torsional actuation amplitude, ft-lb	1.01E+00

**Table A3. Active Twist Rotor structural properties: final design.**

property	description	value	
		( $r/R < 0.27$ )	( $r/R > 0.27$ )
$m$	Section mass per unit length, slug/ft	8.20E-02	1.45E-02
$I_\theta$	Section polar mass moment of inertia, slug-ft <sup>2</sup> /ft	1.18E-04	7.44E-05
$EA$	Axial stiffness, lb	2.20E+06	3.68E+05
$EI_{fw}$	Flapwise stiffness, lb/ft <sup>2</sup>	1.61E+02	9.73E+01
$EI_{cw}$	Chordwise stiffness, lb/ft <sup>2</sup>	3.01E+03	2.65E+03
$GJ$	Torsional stiffness, lb/ft <sup>2</sup>	1.22E+03	8.76E+01
$Q_{PE}$	Maximum piezoelectric torsional actuation amplitude, ft-lb	0	1.01

#### REFERENCES

- Loewy, R., "Recent Developments in Smart Structures with Aeronautical Applications," *Smart Materials and Structures*, Vol. 6, 1997, pp. 11-42.
- Spangler, R. L., Jr. and Hall, S. R., "Piezoelectric Actuators for Helicopter Rotor Control," *AIAA/ASME/ASCE/AHS/ASC 31st Structural Dynamics and Materials Conference, Apr. 2-4, 1990, Technical Papers*, AIAA Paper No. 90-1076, 1990, pp. 1589-1599.
- Samak, D., Chopra, I., "A Feasibility Study to Build a Smart Rotor: Trailing Edge Flap Actuation," *SPIE Smart Structures and Materials Conference, Feb. 1-4 1993, Smart Structures and Intelligent Systems, Proceedings*, Vol. 1917, Part 1, 1993, pp. 225-237.
- Straub, F., "A Feasibility Study of Using Smart Materials for Rotor Control," *Proceedings of the 49th Annual Forum of the American Helicopter Society*, St. Louis, MO, May 1993.
- Millot, T., Friedmann, P., "Vibration Reduction in Helicopter Rotors Using an Actively Controlled Partial Span Trailing Edge Flap Located on the

- Blade," NASA Contractor Report 4611, June 1994.
6. Giurgiutiu, V., Chaudhry, Z., Rogers, C., "Engineering Feasibility of Induced Strain Actuators for Rotor Blade Active Vibration Control," *Journal of Intelligent Material Systems and Structures*, Vol. 6, No. 5, September 1995, pp. 583-597.
  7. Fulton, M., Ormiston, R., "Hover Testing of a Small-Scale Rotor with On-Blade Elevons," Presented at the American Helicopter Society 53rd Annual Forum, Virginia Beach, VA, April 29-May 1, 1997.
  8. Barrett, R., "Intelligent Rotor Blade Structures Development Using Directionally Attached Piezoelectric Crystals," M.S. thesis, University of Maryland, College Park, MD, 1990.
  9. Chen, P., and Chopra, I., "A Feasibility Study to Build a Smart Rotor: Induced Strain Actuation of Airfoil Twisting Using Piezoceramic Crystals," *SPIE Smart Structures and Materials Conference, Feb. 1-4 1993, Smart Structures and Intelligent Systems, Proceedings*, Vol. 1917, Part 1, 1993, pp. 238-254.
  10. du Plessis, A., Hagood, N., "Performance Investigation of Twist Actuated Single Cell Composite Beams for Helicopter Blade Control," presented at the 6th International Conference on Adaptive Structures Technology, Key West, Florida, November 13-15, 1995.
  11. Derham, R., and Hagood, N., "Rotor Design Using Smart Materials to Actively Twist Blades," *American Helicopter Society 52nd Annual Forum Proceedings*, Vol. 2, Washington, D.C., June 4-6, 1996, pp. 1242-1252.
  12. Wilkie, W. Keats, Belvin, W. Keith, Park, K. C., "Aeroelastic Analysis of Helicopter Rotor Blades Incorporating Anisotropic Piezoelectric Twist Actuation," in *ASME 1996 World Congress and Exposition, Adaptive Structures Symposium, Proceedings, Aerospace Division*, November, 1996.
  13. Rodgers, John P., Hagood Nesbitt W., and Weems, Douglas A., "Design and Manufacture of an Integral Twist-Actuated Rotor Blade," AIAA Paper No. 97-1264, presented at 38th AIAA/ASME/AHS Adaptive Structures Forum, Kissimmee, FL, 1997.
  14. Wilkie, W. Keats, "Anisotropic Piezoelectric Twist Actuation of Helicopter Rotor Blades: Aeroelastic Analysis and Design Optimization," Ph. D. thesis, University of Colorado, Boulder, CO, 1997.
  15. Wilkie, W. Keats, Park, K. C., Belvin, W. Keith, "Helicopter Dynamic Stall Suppression Using Active Fiber Composite Rotor Blades," AIAA Paper No. 98-2002, presented at the AIAA/ASME/AHS Structures, Structural Dynamics, and Materials Conference, Long Beach, CA, April 20-23, 1998.
  16. Rodgers, John P., Hagood, Nesbitt W., "Preliminary Mach-Scale Hover Testing of an Integral Twist-Actuated Rotor Blade," presented at SPIE's 5th Annual International Symposium on Smart Structures and Materials, San Diego, California; March 1998.
  17. Rodgers, J. P., Hagood, N. W., "Development of an Integral Twist-Actuated Rotor Blade for Individual Blade Control," AMSL Report #98-6, Active Materials and Structures Laboratory, Massachusetts Institute of Technology, October 1998.
  18. Hagood, N., Kindel, R., Ghandi, K., and Gaudenzi, P., "Improving Transverse Actuation of Piezoceramics Using Interdigitated Surface Electrodes," *SPIE Smart Structures and Materials Conference, Feb. 1-4 1993, Smart Structures and Intelligent Systems, Proceedings*, Vol. 1917, Part 1, 1993, pp. 341-352.
  19. Bent, A., Hagood, N., and Rodgers, J., "Anisotropic Actuation with Piezoelectric Fiber Composites," *Journal of Intelligent Material Systems and Structures*, Vol. 6, May 1995, pp. 338-349.
  20. Bent, A., Hagood, N., "Improved Performance in Piezoelectric Fiber Composites Using Interdigitated Electrodes," SPIE Smart Structures and Materials Conference, February 27-28 1995, *Smart Materials, Proceedings*, Vol. 2441, 1995, pp. 196-212.
  21. Yeager, W., Mirick, P., Hamouda, M-N., Wilbur, M., Singleton, J., Wilkie, W., "Rotorcraft Aeroelastic Testing in the Langley Transonic Dynamics Tunnel," *Journal of the American Helicopter Society*, Vol. 38, No. 3, July 1993, pp.73-82.
  22. *MATLAB Reference Guide*, The MathWorks, Inc., 1992.
  23. Johnson, W., *CAMRAD II, Comprehensive Analytical Model of Rotorcraft Aerodynamics and Dynamics*, Johnson Aeronautics, Palo Alto, California, 1994.

24. Kaza, K. R. V., and Kvaternik, R. G., "Nonlinear Aeroelastic Equations for Combined Flapwise Bending, Chordwise Bending, Torsion, and Extension of Twisted Nonuniform Rotor Blades in Forward Flight," NASA TM 74059, August 1977.
25. Cesnik, Carlos E. S., Shin, SangJoon, "Structural Analysis for Designing Rotor Blades with Integral Actuators," AIAA Paper No. 98-2107, presented at the AIAA/ASME/AHS Structures, Structural Dynamics, and Materials Conference, Long Beach, CA, April 20-23, 1998.
26. Petot, D., "Progress in the Semi-Empirical Prediction of the Aerodynamic Forces Due to Large Amplitude Oscillations of an Airfoil in Attached or Separated Flow," *Proceedings of the Ninth European Rotorcraft Forum*, Stresa, Italy, September 13-15, 1983.
27. Peters, D. A., "Toward a Unified Lift Model for Use in Rotor Blade Stability Analyses," *Journal of the American Helicopter Society*, Vol. 30, No. 3, July, 1985, pp. 32-42.
28. Petot, D., "Differential Equation Modelling of Dynamic Stall," *Recherche Aerospatiale*, Vol. 5, No. 5, 1989.
29. Karunamoorthy, S., Peters, D., "Use of Hierarchical Elastic Blade Equations and Automatic Trim for Rotor Response," *Vertica*, Vol. 11, No. 1/2, 1987, pp. 233-248.
30. Peters, D. A., Chouchane, M., and Fulton, M., "Helicopter Trim with Flap-Lag-Torsion and Stall by an Optimized Controller," *Journal of Guidance, Control and Dynamics*, Vol. 13, No. 5, September-October, 1990, pp. 824-834.
31. Cesnik, E. S., Shin, S. J., Wilkie, W. K., Wilbur, M. L., and Mirick, P. H., "Modeling, Design, and Testing of the NASA/Army/MIT Active Twist Rotor Prototype Blade," *Proceedings of the American Helicopter Society 55<sup>th</sup> Annual Forum*, Montreal, Canada, May 25-27, 1999.